Korean J. Chem. Eng., 34(4), 1159-1169 (2017)
DOI: 10.1007/s11814-016-0357-2

pISSN: 0256-1115
eISSN: 1975-7220

Isotherm, kinetic and thermodynamic studies for Th(IV) sorption by amino group-functionalized titanosilicate from aqueous solutions

Saeid Alamdar Milani* **and Mohammad Karimi****,†**

*Nuclear Fuel Cycle Research School, Nuclear Science and Technology Research Institute, AEOI, P. O. Box 14893-836, Tehran, Iran
**School of Chemical Engineering, College of Engineering, University of Tehran, P. O. Box 11365-4563, Tehran, Iran
(*Received 12 August 2016 • accepted 21 December 2016*)

Abstract−The 3-aminopropyltriethoxysilane-modified titanosilicate was prepared as an alternative for developing efficient adsorbents of heavy metals. The obtained material was characterized by X-ray diffraction analysis, infrared spectroscopy, textural analysis, and scanning electron microscopy. Adsorption of thorium from aqueous solutions was investigated by adsorption isotherms, kinetic and thermodynamic studies. The isothermal data were found to be correlated with the Langmuir model. The maximum sorption capacity of Th(IV) was 83.4 mg g^{-1}. The experimental data show that the external diffusion and intra-particular diffusion are significant in the sorption of thorium. The thermodynamic parameters indicated that the sorption process was physisorption, endothermic and spontaneous.

Keywords: Adsorption, Isotherm, Kinetics, Amino Group-functionalized Titano-silicate, Thermodynamics

INTRODUCTION

Rapid industrialization has led to the increased disposal of heavy metals into the environment. A wide variety of industries are responsible for the release of heavy metals to the water bodies through their wastewater [1,2]. Thorium is one of the toxic heavy metals present in nuclear wastes as a byproduct of the mining of uranium and the manufacture of nuclear fuel, exhibiting a complex behavior in the environment, where it may persist for decades after the source of pollution is stopped. Hence, it is equally important to study the complex phenomena that control the transference of thorium to the environment, and to develop enhanced materials for its removal from the nuclear wastes.

Solvent extraction [3,4], chemical precipitation [5,6], reverse osmosis and membrane processes [7,8], electrodialysis [9], ultrafiltration [10,11], ion exchange [12,13], electro-floatation [14], coagulation [15] and sorption processes [16] are some of the indigenous techniques for removing heavy metal ions from wastewater; and adsorption is considered to be the most suitable and economical method for this purpose [17]. For adsorption of Th(IV) from wastewater, many researchers have used different adsorbents, such as activated carbons [18], gibbsite [19], silica [20], bentonite [21], metallic oxides [22], Pseudomonas sp. [23], Aspergillus fumigatus [24] and perlite [25]. Also, some porous titanosilicates materials have been focused on as adsorbents for long-lived radionuclides in nuclear waste effluents and proven to be promising for environmental remediation [26].

†To whom correspondence should be addressed.
E-mail: m.karimi407@alumni.ut.ac.ir, mohammadkarimi407@gmail.com

Great efforts should be taken to improve sorption process. Several approaches have been studied and among them, functionalization of adsorbents with functional groups (e.g. carboxylates, amino, thiolates, …), have been proven effective in improving the sorption performance of adsorbents as well as reducing the possible drawbacks [27]. Amine functionalized nanotitanate ETS-2 has been successfully used for removing trace-levels of CO_2 from ambient air [28]. The removal of heavy metal ions from aqueous systems by amine-functionalized titanosilicates has also received attention. Amine-functionalized titanosilicates have been used with success for the adsorption of the dyestuff Orange II [29] and for removal of Pb(II), Co(II) and Ni(II) ions [30] from aqueous solutions. However, to the best of our knowledge, no previous studies using amine functionalized titanosilicates as adsorbent have been found in literature at this time for thorium removal from aqueous solutions.

In this work, novel adsorbent material, namely titanosilicate functionalized with 3-aminopropyltriethoxysilane, was synthesized via hydrothermal method route. The obtained material was characterized by X-ray diffraction analysis, infrared absorption spectroscopy, textural analysis, and scanning electron microscopy, and was investigated as an adsorbent for the removal of Th(IV) from aqueous solutions. Adsorption of Th(IV) onto the functionalized titanosilicate has been evaluated in terms of equilibrium, kinetics and thermodynamics studies. The effects of contact time, pH, adsorbent dosage, initial metal concentration, and temperature were investigated. The isotherm models, such as Freundlich, Langmuir, Temkin and Dubinin-Radushkevich isotherm models, have been used to describe the equilibrium data. Kinetic data obtained from the batch adsorption studies were fitted to pseudo-first order, pseudo-second order equations, and intraparticle diffusion model. Furthermore, the adsorption thermodynamic parameters for the adsorption process of Th(IV) ions onto the functionalized titanosilicate

have also been evaluated and discussed.

EXPERIMENTAL

1. Reagents

Tetraethylorthosilicate ($Si(OC_2H_5)_4$, TEOS, 98%), titanium isopropoxide ($Ti(OC_3H_7)_4$, TIP; 99%), 3-Aminopropyltriethoxysilane ($H_2N(CH_2)_3Si(OC_2H_5)_3$, APTES, 99%) were purchased from Sigma-Aldrich. Sodium hydroxide (NaOH; 99.9%), and nitric acid (HNO_3, 63 wt%), were acquired from Merck. Stock solutions of Th(IV) were prepared via the dissolution of appropriate amounts of the $Th(NO_3)_4{\cdot}5H_2O$ (Merck) in distilled water. All working solutions were prepared by diluting the stock solutions with distilled water. NaOH and HNO_3 dilute solutions were used to adjust the desired pH of the aqueous solution.

2. Instrumentation

The phase of synthesized samples was identified by X-ray diffraction (XRD, Philips PW1800, Netherlands) technique using Cu$K\alpha$ radiation (λ=1.5406 A°).

BET surface area, pore volume, pore size distribution and pore radius were determined by nitrogen adsorption-desorption at 77 K in relative pressure range 0.002-0.99 using Nova Win software provided with Quantachrome Nova 2200e surface area and pore size analyzer.

Infrared adsorption spectroscopy involved a Perkin-Elmer Model 1739 spectrometer with Fourier transform, for more confirmation of surface modification of titanosilicate by APTES coating and to assess functional groups on the surface of titanosilicate products. Both nonfunctionalized titanosilicate and functionalized titanosilicate were analyzed by FT-IR between 4,000 and 400 cm^{-1}. Consequently, dried powders were mixed with KBr powder and then pressed to produce pellets.

The samples size and morphology were investigated by scanning electron microscope (SEM, Cambridge S360). All spectrophotometric measurements were by Varian Liberty 220 inductively coupled plasma optical emission (Varian Mulgrave, Australia). The pH measurements and adjustments were carried out using a Metrohm 713 pH-meter equipped with a combined glass electrode.

3. Preparation of APTES Modified Titanosilicate

The used titanosilicates were synthesized by the hydrothermal method. To this end, in a beaker, 3.53 ml of tetraethyl orthosilicate as well as 3.44 ml titanium isopropoxide was added to 50 ml of solution containing 12.64 g sodium hydroxide and stirred magnetically for 1 hour. The obtained white solution was heated at 443 K for four days using a 100 ml Teflon-lined stainless steel autoclave. The resulting precipitate was separated from the reaction medium by centrifugation, washed with deionized water several times and dried overnight in a vacuum oven at 343 K. In the second step, a weighed amount of the obtained product was dissolved in distilled water and ultrasonicated (Bandelin SONOPULS HD2200, Germany) for about an hour. Subsequently, APTES with different % weight (0 to 40%) was added and stirred for 20 hours. Then the derived precipitate was separated in a centrifuge and dried overnight in a vacuum oven at 323 K. The product obtained was denoted as $TiSiNH_2$. Optimal $TiSiNH_2$ content of APTES was determined through a series of batch experiments of the Th(IV) adsorption by 1 g L^{-1} of $TiSiNH_2$ as an adsorbent, with the Th(IV) initial concentration of 100 mg L^{-1} at room temperature.

4. Adsorption Equilibrium Studies of Th(IV)

Batch adsorption experiments were performed to study the effects of solution pH, initial Th(IV) ion concentration, the dosage of adsorbent, and temperature on optimization of Th(IV) adsorption. The concentration of Th(IV) ion before and after equilibrium adsorption was measured by using an ICP-OES at the wavelength of 401.913 nm. The adsorption capacity was defined according to [16]:

$$q_e = \frac{(C_o - C_e)V}{m} \quad (1)$$

where q_e (mg g^{-1}) is the equilibrium adsorption capacity; C_e and C_o (mg L^{-1}) are the equilibrium and initial metal ion concentrations, respectively; m and V are the weight of dried used adsorbent (g) and the liquid volume (L).

Adsorption experiments of Th(IV) onto $TiSiNH_2$ were in flasks

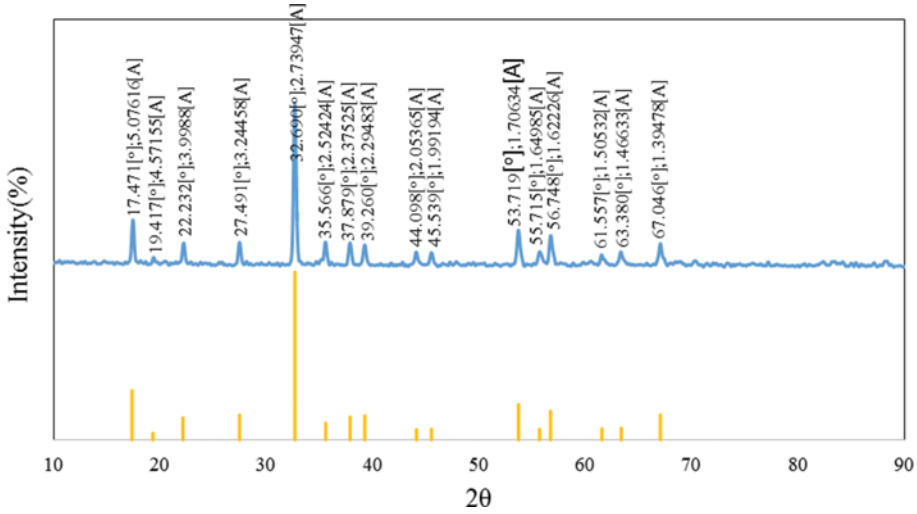

Fig. 1. XRD pattern of (a) freshly prepared titanosilicate and (b) reference titanosilicate.

containing 100 mL Th(IV) solution by shaking the flasks at 150 rpm at a period contact time of 20 h (unless otherwise stated).

RESULTS AND DISCUSSION

1. Characterization of the Adsorbent

The XRD pattern of the prepared samples was compared with the standard values of nano-titanosilicate from JCPDS files (JCPDS no. 86-1615). The observed values were in good agreement with the standard values, and the observed XRD pattern (Fig. 1) was similar to the earlier report [31]. The XRD pattern indicates the formation of crystalline titanosilicate with the mineral natisite topology. The sharp diffraction peaks indicate good crystallinity of the prepared particles and no evidence of bulk remnant materials and impurity. The average crystallite size was tentatively calculated from XRD peak width of (201) based on the Debye-Scherrer Eq. (2) [32].

$$\tau = \frac{K\lambda}{\beta \cos\theta} \quad (2)$$

where K is the shape factor, λ is the X-ray wavelength, typically 1.54 Å (0.15406 nm in our case), β is the line broadening at half the maximum intensity (FWHM) in radians and θ is the Bragg angle [33] τ is the mean size of the ordered (crystalline) domains, which may be smaller or equal to the grain size. The dimensionless shape factor has a typical value of about 0.9, but varies with the actual shape of the crystallite. The Scherrer equation is limited to nanoscale particles. It is not applicable to grains larger than about 0.1 μm, which precludes those observed in most metallographic and ceramographic microstructures.

The average crystallite size corresponding to this pattern is ~25 nm. The average particle sizes of the prepared samples were calculated from Eq. (2) to be ~25 nm. The surface morphology of freshly prepared titanosilicate is shown in the SEM images (Fig. 2). In the SEM image, the particles consist of agglomerated nanoparticles. The chemical composition of sample was evaluated using EDX spectra. Fig. 3 shows the EDX spectra for freshly prepared titanosilicate nanoparticles. The spectra obtained from EDX analysis qualitatively confirmed the purity of investigated titanosilicate powder. The atomic weight ratio of Na : Si : Ti was 22 : 31 : 47.

Surface area values of the adsorbent materials, as well as pore volume data, are presented in Table 1. The surface area was calculated by the BET method, while the total pore volume was determined from the amount of nitrogen adsorbed at the highest relative pressure p/p_o=0.99. Pore volume was calculated using the Dubinin-Radushkevich (D-R) equation [34] and the pore size by Dubinin-Astakov (D-A) method [35].

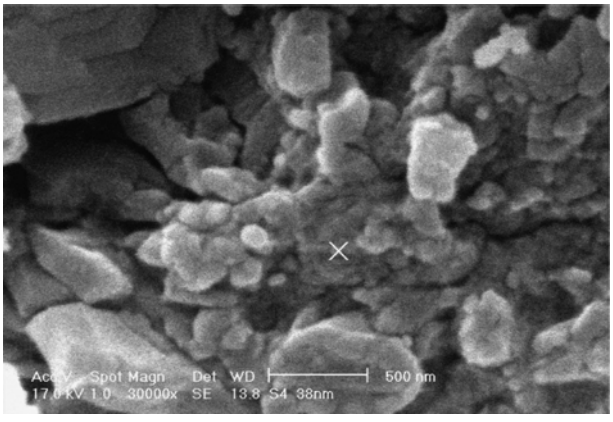

Fig. 2. SEM micrograph of freshly prepared titanosilicate.

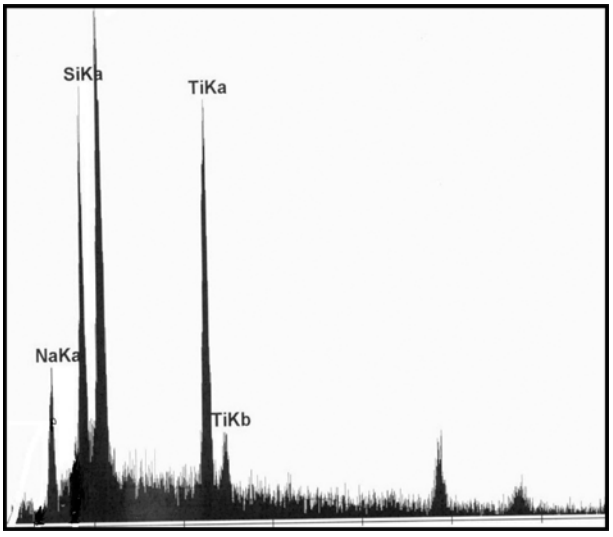

Fig. 3. EDX spectrum of freshly prepared titanosilicate nanoparticles.

Table 1. Textural properties of $TiSiNH_2$

BET surface area ($m^2\ g^{-1}$)	Pore volume ($cm^3\ g^{-1}$)	Average pore diameter (nm)
122.234	0.088	1.422

The functional groups in the samples were identified by the comparison of FT-IR data of non-APTES grating sample with those of APTES-functionalized sample. The reference spectrum of APTES [36] is reported in Fig. 4. Fig. 5 shows the FT-IR spectra of the resulting functionalized titanosilicate nanoparticles as compared to the starting materials. The FT-IR spectrum of the non-functionalized sample showed a broad band at 3,200-3,500 cm^{-1} (indicating O-H stretch vibration), a number of absorption peaks at 994, 926, 867 and 728 cm^{-1} (corresponding to the Si-O, Si-O-Ti, Ti-O-Ti and Ti-O stretch vibration, respectively), and a peak at 451 cm^{-1} (ascribed to the Si-O-Si bending) [37-39]. The FT-IR spectrum of the APTES-functionalized sample showed a new peak at 2,900 cm^{-1} (indicating stretch vibration of C-H bond of functionalized titanosilicate) and two new peaks at 1,639 and 1,382 cm^{-1} (relating to bending of NH_2 functional group and HCH bond, respectively). Furthermore, two new peaks at 3,365 cm^{-1} and 3,257 cm^{-1} overlapping the broad band at 3,200-3,500 cm^{-1} (corresponding to O-H stretch vibration, as mentioned above). On the other hand, the peak at 750-780 cm^{-1} (indicating the Si-OH vibration) that was observed in the non-APTES-functionalized sample disappeared in the APTES-functionalized sample. Anbia et al. [40] reported that these groups are very sensitive to functionalization, since this process occurs via the condensation of Si-OH or Ti-OH groups, hydrolyzed together with

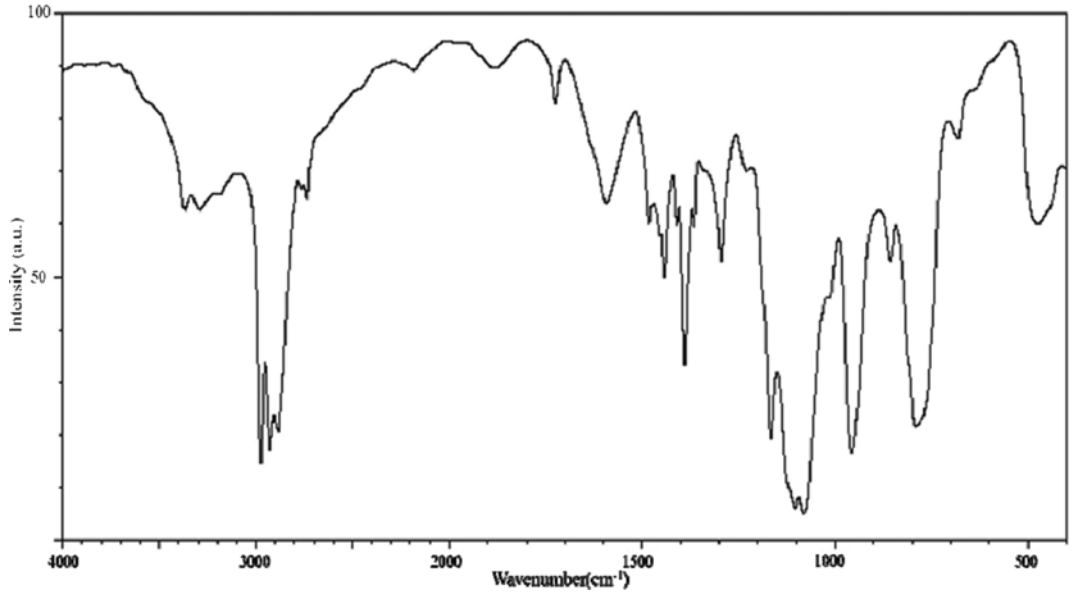

Fig. 4. Infrared spectra of the APTES.

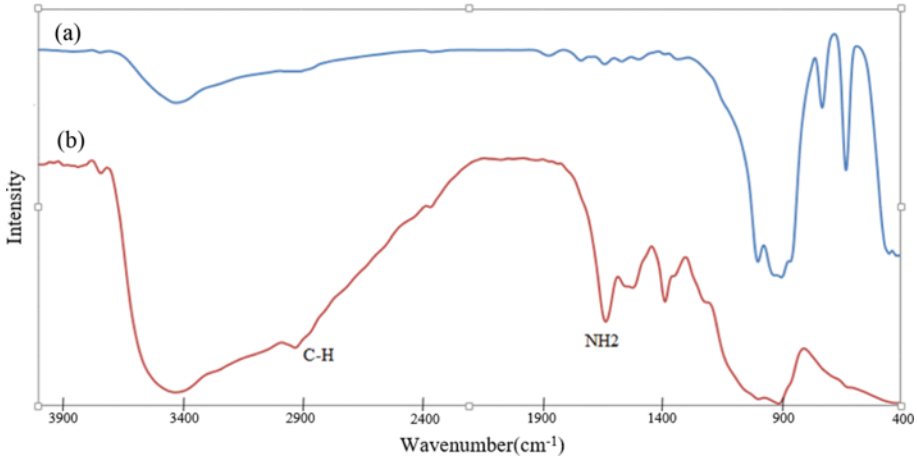

Fig. 5. Infrared spectra of freshly prepared titanosilicate (a) and functionalized titanosilicate (b).

the alkoxide molecules (Fig. 6). The strong absorption in the regions of 3,600 and 1,600 cm^{-1} is characteristic of the -OH groups, the hydrophilic NH_2 groups induce the adsorption of water (and/or the solvent) molecules remaining from the synthesis medium. These FT-IR results suggest that APTES was successfully deposited on the titanosilicate surface.

2. Effect of APTES Content

The effect of APTES content on Th(IV) adsorption was examined at different APTES/titanosilicate weight percentages (0-50 wt% with respect to the titanosilicate weight) at pH, adsorbent dosage, initial Th(IV) concentration, contact time and temperature of 4.5, 1 g L^{-1}, 100 mg L^{-1}, 5 h and 298 K, respectively. The sorption capacity of the adsorbent for the adsorbate is shown in Fig. 7. The sorption capacity increases with the increase of APTES amount up to 10 wt%. This increase is due to more uniform surface and more regular pore structure. Further increase in the APTES content decreases the sorption capacity. This reduction can be due to a decrease in surface area and pore volume reducing the active sites of $TiSiNH_2$ for the sorption process. However, $TiSi10\%NH_2$ material was selected for further studies.

3. Optimization of Th(IV) Adsorption

3-1. Effect of Solution pH

The pH of the aqueous medium is an important factor that is apt to influence the adsorbate uptake; the pH of the solution affects the degree of ionization and speciation of metallic ion. The adsorption of Th(IV) ion by $TiSiNH_2$ was investigated with pH ranging from 2.0 to 6.0 by keeping other variables constant (at adsorbent dose=3.5 g L^{-1}, initial concentration of Th(IV) solution=150 g L^{-1}, contact time=1,200 min, temperature=308 K and shaker speed=150 rpm). The experimental results are presented in Fig. 8. The adsorption capacity increased with the pH ranging from 2.0 to 4.5. Also, a total decrease of the adsorption capacity was observed under acidic conditions, which could be due to the protonation of the sulfonate groups, causing repulsion between the amino groups of

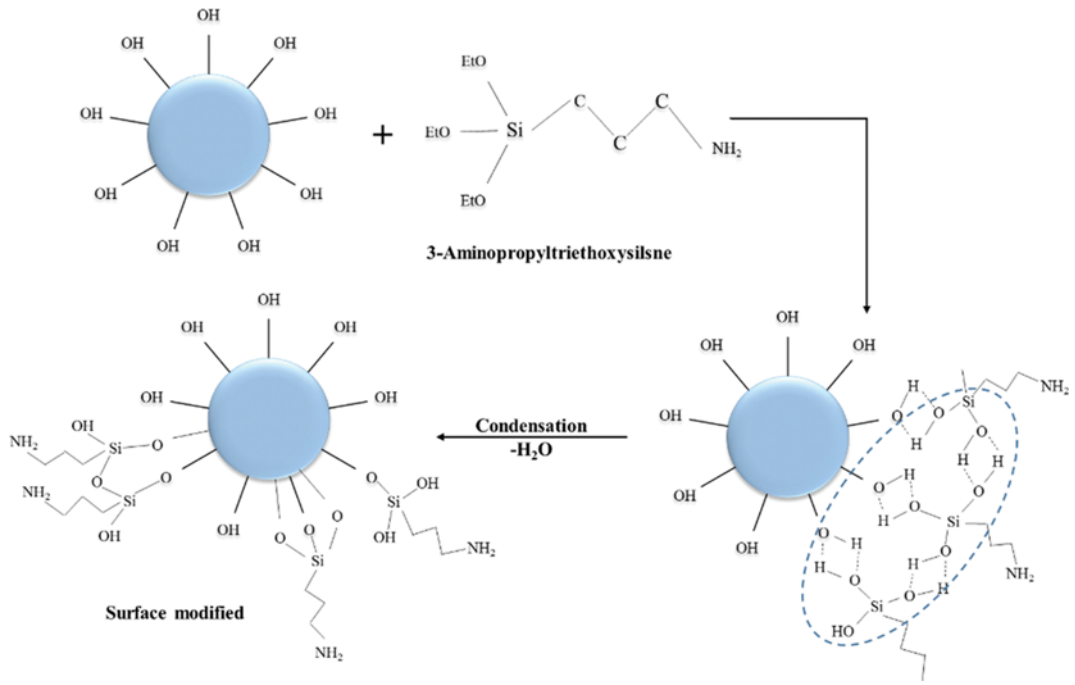

Fig. 6. Main interactions between titanosilicate and APTES.

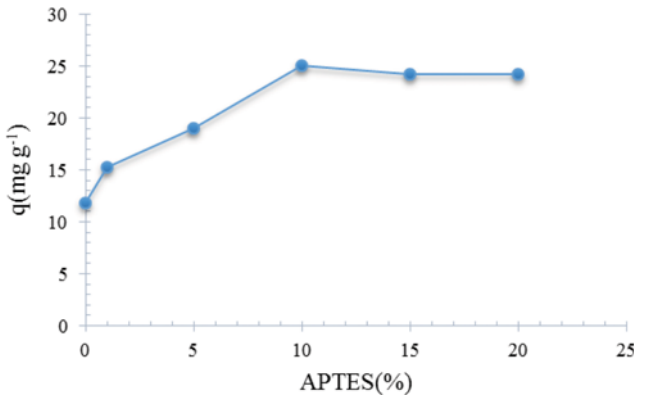

Fig. 7. Effect of adsorbent's APTES content on Th(IV) adsorption (pH, 4.5; initial thorium solution concentration, 100 mg L^{-1}; $t_{contact}$, 1,200 min; dosage, 1 g L^{-1}; temperature, 298 K; shaker speed, 150 rpm).

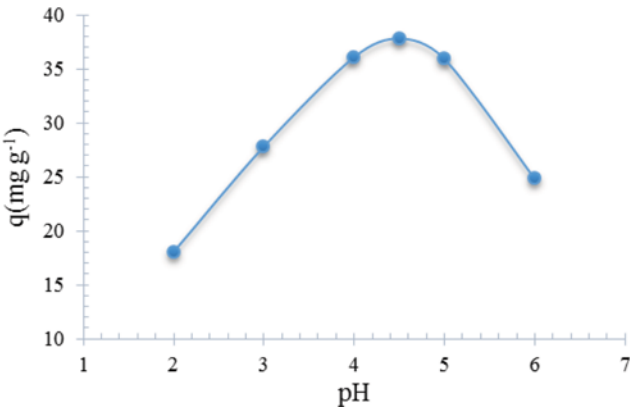

Fig. 8. Effect of pH value of Th(IV) solution on adsorption (initial thorium solution concentration, 150 mg L^{-1}; dosage, 3.5 g L^{-1}; temperature, 308 K; $t_{contact}$, 1,200 min and shaker speed, 150 rpm).

the adsorbent, which were probably protonated. Moreover, at low pH a competition for the active sites of the adsorbent between Th(IV) ions and protons in the acid media may be proposed, and the different affinity of the adsorbent for these species can be responsible for the behavior observed. Also, the adsorption decreases when pH is above 4.5, albeit explicable on the basis of the formation of different thorium species with lower adsorption affinities for the surface sites, such as $[Th_2(OH)_2]^{6+}$, $[Th_3(OH)_5]^{7+}$, $[Th_4(OH)_8]^{8+}$, and $[Th_6(OH)_{15}]^{9+}$ [41,42].

3-2. Effect of Adsorbate Concentration

The effect of initial concentration of adsorbate on the adsorption process was analyzed within the range 25-550 mg L^{-1} (Fig. 9). As shown in Fig. 9, when the adsorbate concentration increases from 25 to 550 mg L^{-1}, the adsorption capacity increases due to the increasing driving force of the mass transfer and occupying the available active sites on the adsorbent by Th(IV) ions.

3-3. Effect of Adsorbent Dose

The effect of initial concentration of adsorbate on the adsorption process was analyzed within the range 25-550 mg L^{-1} (Fig. 9). As shown in Fig. 9, when the adsorbate concentration increases from 25 to 550 mg L^{-1}, the adsorption capacity increases because of the increasing driving force of the mass transfer and occupying the available active sites on the adsorbent by Th(IV) ions.

3-4. Effect of Adsorbent Dose

Adsorbent dose variation experiment is one of the significant parts of the study that determines the capacity of the adsorbent for

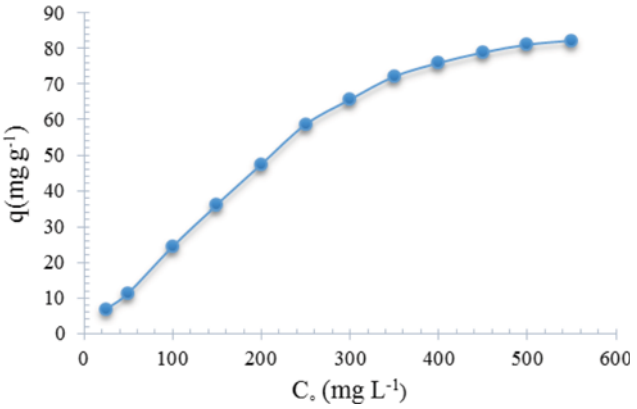

Fig. 9. Effect of initial concentration on adsorption of Th(IV) (pH, 4.5; $t_{contact}$, 1,200 min, dosage, 3.5 g L^{-1}; temperature, 318 K; shaker speed, 150 rpm).

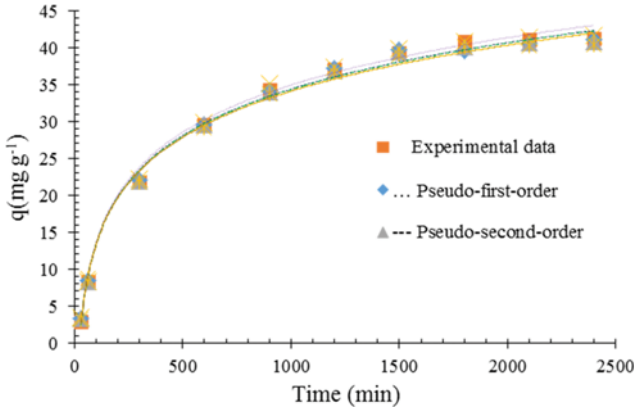

Fig. 11. Adsorption kinetics of thorium onto the $TiSiNH_2$ (initial concentration, 175 mg L^{-1}; pH, 4.5; temperature, 318 K; dosage, 3.89 g L^{-1} and shaker speed, 150 rpm).

a given initial concentration of Th(VI) in the operating circumstances. Thus, the experiments varied adsorbent doses only in the range 1-5 g L^{-1} by keeping other variables constant (at optimal pH of 4.5, initial concentration of Th(IV) solution=150 g L^{-1}, contact time=1,200 min, temperature=308 K, and shaker speed=150 rpm). After the adsorption time had been completed the adsorbents were removed from the solution and the concentration of the residual metal ion in each solution was determined by means of ICP-OES. The effect of the adsorbent dose on the adsorption of Th(IV) is shown in Fig. 10. As illustrated, the adsorption capacity of TiSiNH2 presents a declining trend as the dosage increases; the phenomenon may be attributed to the decrease in active sites and agglomeration of the adsorbents. With the increasing of the adsorbent dosage, the active sites of adsorbents provided are greatly more than the saturated threshold adsorption point; thus, only a part of the active sites are occupied by Th(IV), leading to the decrease of adsorption capacity [43]. In addition, a higher adsorbent amount creates particle aggregation, resulting in a decrease in the total surface area and an increase in diffusional path length, both of which contribute to decrease in amount adsorbed per unit mass [44].

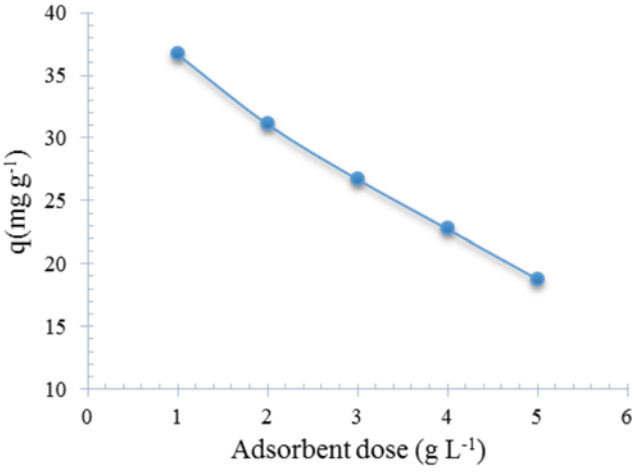

Fig. 10. Effect of adsorbent dose on the adsorption of Th(IV) on $TiSiNH_2$ (initial concentration of Th(IV) solution, 150 mg L^{-1}; pH, 4.5; temperature, 308 K; $t_{contact}$, 1,200 min and shaker speed, 150 rpm).

3-5. Kinetic Studies on the Sorption of Th(IV) onto $TiSiNH_2$

Fig. 11 shows the adsorption kinetic curve of Th(IV) from a 175 mg L^{-1} solution with pH 4.5 onto 3.89 g L^{-1} $TiSiNH_2$ at 318 K. The results demonstrated that the adsorption procedure was generally consistent with the three-step adsorption behavior usually observed in porous adsorbents [45]. Initially, the adsorption rate was fast and then decreased over time, after about 1,500 minutes, the adsorption reached equilibrium at about 30 h. This adsorption behavior was attributed to the fact that at the beginning, the adsorption of Th(IV) onto the adsorbent mainly occurred on the external surface of adsorbent and the adsorption rate was rapid. Then, the concentration of Th(IV) began to decrease over time as adsorption progressed. Meanwhile, the adsorbed Th(IV) ions diffused inward into the adsorbent through the micropore, and the resistance of diffusion increased. The adsorption rate was mainly controlled by diffusion at this stage, so the rate of adsorption was reduced. At the final stage, the adsorption mainly occurred on the inner surface of the adsorbent while the concentration of Th(IV) in the solution was reduced, and the adsorption reached equilibrium at the last stage. Adsorption kinetics analysis indicated that 1,500-1,800 minutes was sufficient to attain equilibrium.

To investigate the adsorption mechanism and rate controlling steps, the adsorption kinetic data were modeled according to pseudo-first-order and pseudo-second-order rate equations, intraparticle diffusion, and double exponential kinetic equations [46,47]:

Pseudo-first-order model: $$q_t = q_e(1-\exp(-k_1 t)) \quad (3)$$

Pseudo-second-order model: $$q_t = \frac{k_2 q_e^2 t}{1+k_2 q_e^2} \quad (4)$$

Intra-particle diffusion model: $$q_t = k_i t^{1/2} + C_i \quad (5)$$

Double-exponential model:

$$q_t = q_e - \frac{D_1}{m_{ads}}\exp(-k_{D_1} t) - \frac{D_2}{m_{ads}}\exp(-k_{D_2} t) \quad (6)$$

where q_e and q_t are the adsorbent capacities (mg g^{-1}) for the metal

Table 2. Rate constants for Th(IV) adsorption onto the $TiSiNH_2$

q_{exp} (mg g^{-1})	Pseudo-first-order model						
	k_1 (min^{-1})		q_e (mg g^{-1})		R^2		
40	0.0024		40.44		0.9897		
	Pseudo-second-order model						
	k_2 (g mg^{-1} min^{-1})		q_e (mg g^{-1})		R^2		
40	0.00008		44.98		0.9935		
	Intra-particle diffusion model						
	k_i (g mg^{-1} min^{-1})		C		R^2		
40	0.8794		3.6435		0.9272		
	Double-exponential kinetic model						
	D_1 (g L^{-1})	D_2 (g L^{-1})	k_{D_1} (min^{-1})	k_{D_2} (min^{-1})	m_{ads} (g L^{-1})	q_e (mg g^{-1})	R^2
40	8.28	3.91	0.0016	0.021	0.2573	42.07	0.9997

at equilibrium and at time t, respectively; k_1 (min^{-1}) is the pseudo-first-order rate constant; k_2 (g mg^{-1} min^{-1}) is the pseudo-second-order rate constant; k_i (mg g^{-1} min^{-1}) is the intra-particle diffusion constant at stage i and C_i is the intercept at stage i, and the value of C_i is related to the thickness of the boundary layer; and D_1 and D_2 (g L^{-1}) are the equation constants which correspond to the rapid and slow phases, respectively. k_{D_1} and k_{D_2} (min^{-1}) are the double-exponential rate constants and m_{ads} (g L^{-1}) is the adsorbent dose.

The parameters of the kinetic models, which were calculated by plotting q_t versus t (Fig. 11), are given in Table 2. A good correlation between the experimental data and the double-exponential rate kinetic model (R^2>0.999) was obtained. Therefore, as mentioned, the adsorption procedure in this study occurs in two steps: the external diffusion (transport of the Th(IV) ion to the external surface of the adsorbent) which is a rapid phase and the internal diffusion (adsorption of the Th(IV) ion on the inner surface of the adsorbent), which is a slow phase.

3-6. Sorption Isotherms of Th(IV)

The experimental data obtained from the effect of the initial Th(IV) ion concentrations were used to test the different adsorption isotherm models: Freundlich, Langmuir, Temkin and Dubinin-Radushkevich. Adsorption isotherms are the basic requirements for designing any adsorption system. The adsorption isotherm is used to find the relationship between the equilibrium concentration of the adsorbate in the liquid and solid phase. The adsorption isotherm of Th(IV) ions onto $TiSiNH_2$ was studied in various concentrations of Th(IV) ion solutions from 50 to 400 mg L^{-1} at 318 K.

The Langmuir model is based on monolayer, uniform, and finite adsorption site assumptions. The linear form of the Langmuir isotherm model is expressed as the following equation [48]:

$$\frac{C_e}{q_e} = \frac{1}{K_L q_m} + \frac{C_e}{q_m} \quad (7)$$

where C_e is the equilibrium concentration of the remaining metals in the solution (mg L^{-1}); q_{max} is the amount of the adsorbate to form complete monolayer coverage (mg g^{-1}); K_L is the Langmuir isotherm constant (L mg^{-1}) relevant to the heat of adsorption. The

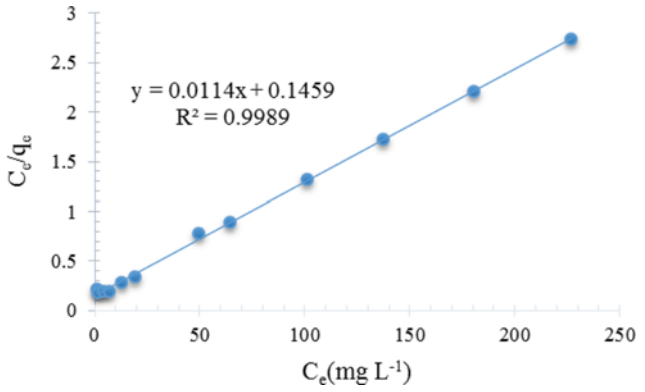

Fig. 12. Langmuir isotherm for Th(IV) adsorption onto the $TiSiNH_2$ at 318 K.

Table 3. Isotherm model parameters for Th(IV) adsorption onto $TiSiNH_2$

Isotherm	Parameter	
Langmuir	q_{max} (mg g^{-1})	87.71
	K_L (L mg^{-1})	0.08266
	R^2	0.9989
Freundlich	K_F (mg g^{-1} (L $mg^{-1})^n$)	14.489
	n	0.4007
	R^2	0.9058
D-R	q_m (mmol g^{-1})	0.4008
	β (mol^2 j^{-2})	1.32×10^{-8}
	E (kj mol^{-1})	6.153
	R^2	0.9764
Temkin	b_T (j mol^{-1})	168.915
	K_T (L g^{-1})	1.2753
	R^2	0.9773

Langmuir constants q_{max} and K_L were determined from the slope and intercept of the plot of specific sorption (C_e/q_e) against the equilibrium concentration (C_e) (Fig. 12), which are presented in

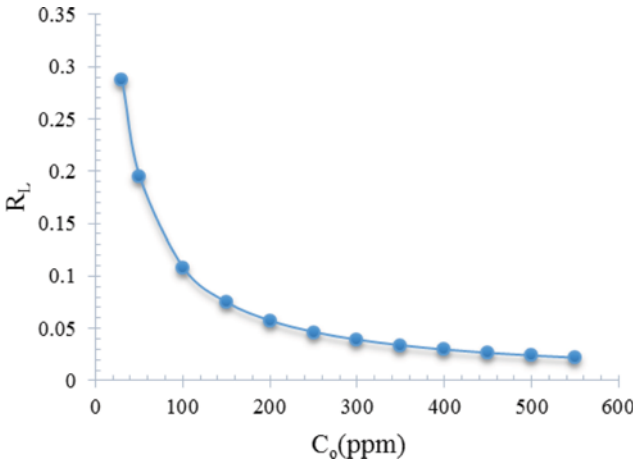

Fig. 13. Plot of separation factor versus initial Th(IV) concentration.

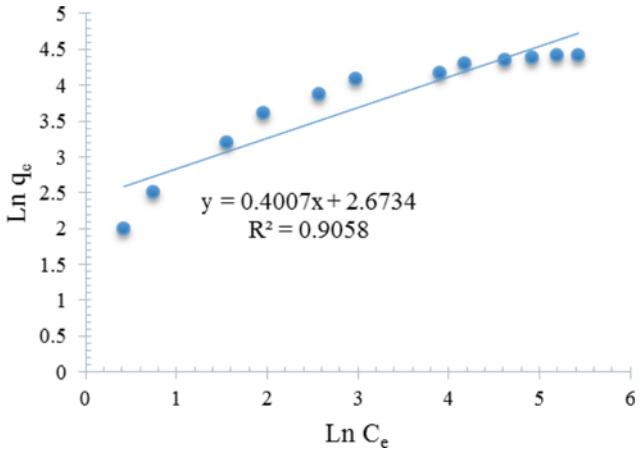

Fig. 14. Freundlich isotherm for Th(IV) adsorption onto the TiSiNH$_2$ at 318 K.

Table 3.

The essential characteristics of the Langmuir isotherm may be expressed in terms of a dimensionless constant separation factor or equilibrium parameter R_L that is given by the following equation:

$$R_L = \frac{1}{1 + K_L C_o} \quad (8)$$

where C_o is the initial concentration, K_L is the constant related to the energy of adsorption (Langmuir constant). R_L value indicates the adsorption nature to be either unfavorable if R_L>1, linear if R_L=1, favorable if 0<R_L<1 and irreversible if R_L=0. Fig. 13 shows the variation of separation factor (R_L) with initial Th(IV) solution concentration. The R_L values were in the range of 0-1 at 318 K, indicating that the sorption of Th(IV) onto TiSiNH$_2$ is favorable. Also, the R_L value approaches zero with the increase of C_o which means that the sorption of Th(IV) on functionalized titanosilicate is less favorable at high initial Th(IV) concentration.

The Freundlich isotherm can be applied for non-ideal sorption on heterogeneous surfaces and multilayer sorption. The Freundlich equation is expressed as [48]:

$$q_e = K_F C_e^n \quad (9)$$

where K_f and n are Freundlich constants with K_f (mg g^{-1} (L mg^{-1})^n) being the sorption capacity of the adsorbent, and n giving an indication of the favorability of the sorption process. Values of n>1 represent favorable adsorption condition [49]. To determine the constants K_f and n, the Freundlich equation can be described by the linearized form:

$$\ln q_e = \ln K_F + \frac{1}{n} \ln C_e \quad (10)$$

Values of K_f and n are calculated from the intercept and slope of the linear plot of Freundlich isotherm of Th(IV) sorption onto TiSiNH$_2$ at 318 K (Fig. 14), as are presented in Table 3.

Temkin and Pyzhev considered the effects of some indirect adsorbate/adsorbate interaction on adsorption isotherms and suggested that because of these interactions the heat of adsorption of all the molecules in the layer would decrease linearly with coverage [50]. The Temkin isotherm has been generally applied in the following form:

$$q_e = \left(\frac{RT}{b_T}\right) \ln(K_T C_e) \quad (11)$$

and can be linearized as:

$$q_e = B \ln A + B \ln C_e \quad (12)$$

where B=RT/b_T, b_T is the Temkin constant related to heat of sorption (J mol^{-1}), K_T is the Temkin isotherm constant (L g^{-1}), R is the gas constant (8.314 J mol^{-1} K^{-1}), and T is the absolute temperature (K). The constants A and B are calculated from the intercept and slope of the linear plot of Temkin isotherm of Th(IV) sorption on TiSiNH$_2$ at 318 K (Fig. 15) as listed in Table 3.

The equilibrium data were also applied to the D-R model [51-53] to determine the type of sorption (physical or chemical). The linear form of D-R isotherm is presented as the following equation:

$$\ln q_e = \ln q_m - \beta \varepsilon^2 \quad (13)$$

where q_e is the amount of the adsorbate adsorbed onto per unit dosage of the adsorbent (mol g^{-1}), q_m is the theoretical monolayer sorption capacity (mol g^{-1}), β is the constant of the sorption energy (mol^2 J^{-2}), which is related to the average energy of sorption per

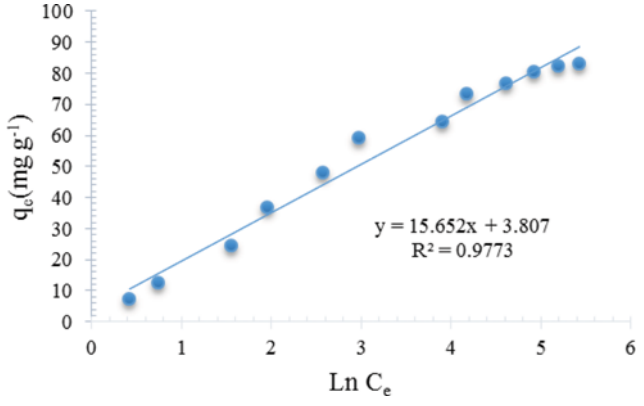

Fig. 15. Temkin isotherm for Th(IV) adsorption onto the TiSiNH$_2$ at 318 K.

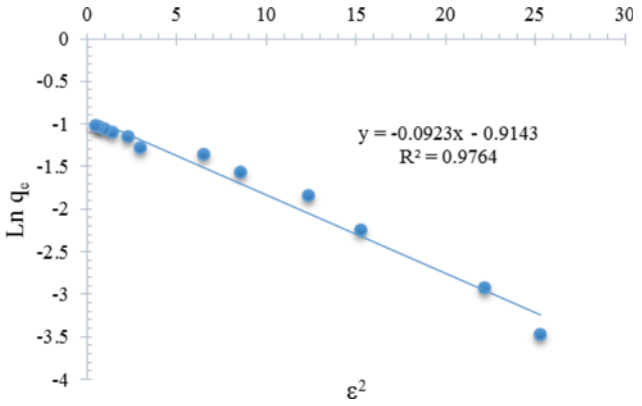

Fig. 16. D-R isotherm for Th(IV) adsorption onto the $TiSiNH_2$ at 318 K.

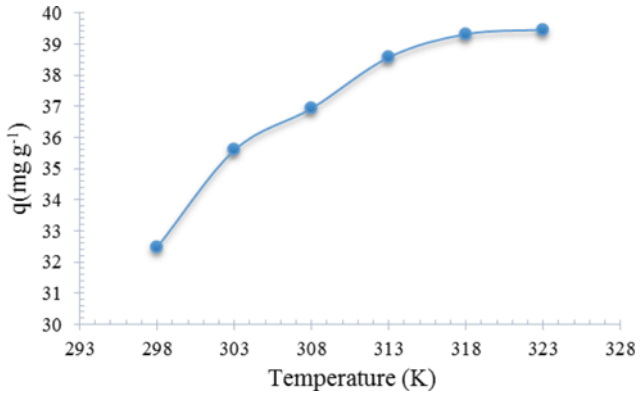

Fig. 17. Effect of temperature on Th(IV) removal onto $TiSiNH_2$ (Th (IV) ion concentration, 150 mg L^{-1}; dosage, 3.5 g L^{-1}; pH 4.5, temperature 298-318 K, equilibrium time 1,200 min and shaker speed, 150 rpm).

mole of the adsorbate as it is transferred to the surface of the solid from the infinite distance in the solution [52,54], and ε is Polanyi potential, which is described as

$$\varepsilon = RT\ln\left(1+\frac{1}{C_e}\right) \tag{14}$$

where T is the solution temperature (K) and R is the gas constant and is equal to 8.314 J $mol^{-1}K^{-1}$. The value of mean sorption energy, E (kJ mol^{-1}), can be calculated from D-R parameter β as follows:

$$E = \frac{1}{\sqrt{-2\beta}} \tag{15}$$

The value of mean sorption energy gives information about chemical and physical sorption. The E value ranges from 1 to 8 kJ mol^{-1} for the physical sorption and from 8 to 16 kJ mol^{-1} for the chemical sorption [52,54].

Values of q_m, β and E are calculated from the intercept and slope of the plot of ln q_e versus ε^2 (Fig. 16), which are listed in Table 3.

As seen in Table 3, the Langmuir isotherm fits quite well with the experimental data (correlation coefficient R^2>0.998). This fact indicates that the Langmuir model was very suitable for describing the sorption equilibrium of Th(IV) on $TiSiNH_2$. The maximum sorption capacity of $TiSiNH_2$ for Th(IV) was 87.71 mg g^{-1} at 318 K. The fact that the Langmuir isotherm fits the experimental data very well may be due to the homogeneous distribution of active sites on $TiSiNH_2$ surface, since the Langmuir equation assumes that the surface is homogeneous. Compared with the correlation coefficient value of the linear plot of Langmuir isotherm, those of Freundlich model, Temkin model, and D-R model were found less satisfactory (R^2<0.98). The E value (6.153 kJ mol^{-1}) was found in the range of 1 to 8 kJ mol^{-1}, indicating that the type of sorption of Th(IV) on $TiSiNH_2$ is essentially physical.

4. Adsorption Thermodynamics

The effect of temperature on the removal of Th(IV) ions from the aqueous solution using the amino group-functionalized titanosilicate ($TiSiNH_2$) was studied by doing the batch adsorption experiments for an initial Th(IV) ions concentrations of 150 mg L^{-1} at a constant dose of 3.5 g L^{-1} and at a temperature of 293-323 K for 1,200 min, the result of which is shown in Fig. 17. The equilibrium adsorption capacity of $TiSiNH_2$ for Th(IV) ions increases from 32.48 to 39.32 mg g^{-1} with increasing temperature from 293 to 323 K. This is mainly due to the increase in surface activity, suggesting that the adsorption between Th(IV) ions and $TiSiNH_2$ is endothermic. When the temperature increased, solute movement became faster and the collision frequency between the solute and absorbent surface became higher, thus increasing sorption. The maximum removal of Th(IV) ions was obtained at 323 K.

To consider the thermodynamic behavior of the adsorption of Th(IV) ions onto the $TiSiNH_2$, thermodynamic parameters such as change in Gibbs free energy (ΔG^o), enthalpy change (ΔH^o), and entropy change (ΔS^o) were estimated using equilibrium constants changing with temperature. The Gibbs free energy change of the adsorption reaction is given by the following equation:

$$\Delta G^o = -RT\ln(K_c) \tag{16}$$

where K_C is the adsorption equilibrium constant that was calculated by the ratio of amount of adsorbate adsorbed (q_e) to the amount remaining in the solution (C_e):

$$K_C = \frac{q_e}{C_e} \tag{17}$$

Based on the above equations, the following van't Hoff equation can be derived:

$$\ln(K_C) = \frac{\Delta S^o}{R} - \frac{\Delta H^o}{RT} \tag{18}$$

ΔH^o and ΔS^o were obtained from the slope and intercept of the plot of ln K_c versus 1/T. The van't Hoff plot for the adsorption of Th(IV) onto $TiSiNH_2$ is shown in Fig. 18, and the thermodynamic parameters calculated are summarized in Table 4. The positive value of ΔH^o and negative values of ΔG^o confirm the endothermic and spontaneous nature of the adsorption process. The change in free energy generally ranges from −80 to −400 kJ mol^{-1} for chemisorption, from −20 to −80 kJ mol^{-1} for physicochemical process and from −20 to 0 kJ mol^{-1} for physisorption [55]. The calculated ΔG^o values indicate that the sorption of Th(IV) ions onto the adsorbent is a physisorption process. Basically, the heat evolved during physical sorption is of the same order of magnitude as the heat of

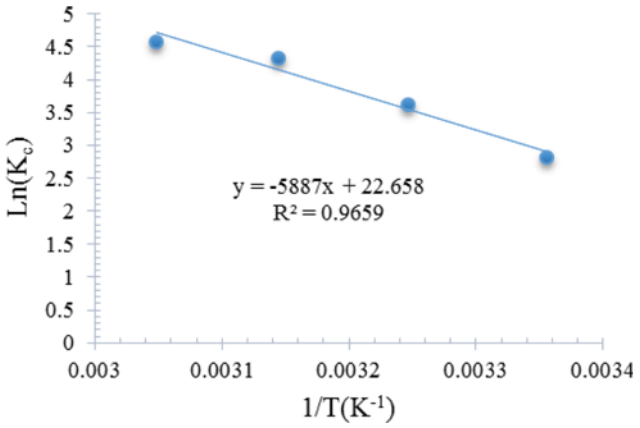

Fig. 18. Van't Hoff plot for the thorium adsorption on $TiSiNH_2$.

Table 4. Thermodynamic parameters for Th(IV) adsorption onto the $TiSiNH_2$

ΔS^o	ΔH^o	ΔG^o (kJ mol^{-1})			
(J mol^{-1}K^{-1})	(kJ mol^{-1})	298 K	308 K	318 K	328 K
188	48.94	−7.084	−8.964	−10.844	−12.724

condensation, 2.1-20.9 kJ mol^{-1} [55], while the heat of chemisorption generally falls into a range of 80-200 kJ mol^{-1} [56]. Therefore, it seems that thorium sorption by $TiSiNH_2$ would be attributed to a physicochemical sorption process rather than a pure physical or chemical sorption process. Also, the low value of ΔS^o may imply that no remarkable change in entropy occurs during the sorption of Th(IV) by the $TiSiNH_2$. In addition, the positive value of DS^o reflects the increased randomness at the solid-solution interface during sorption, and it also indicates an affinity of the sorbent with thorium. Normally, adsorption of gases leads to a decrease in entropy due to orderly arrangement of the gas molecules on a solid surface. However, the same may not be true for the complicated system of sorption from solution onto $TiSiNH_2$.

5. Application to Real Samples

To verify the applicability of the developed sorbent in the removal of Th(IV) ions, it was applied to extraction of Th(IV) ions in a real sample. In this study, the real waste-water sample was collected from uranium conversion facility (UCF), Esfahan, Iran. The characteristics of the waste-water sample are presented in Table 5. No Th(IV) ions were found in the tested waste-water, so 100 mL of the waste-water sample spiked with 300 μg mL^{-1} Th(IV) ions was treated by the sorption procedure as described in the experimental section. The pH of the waste-water sample was about 5. Adsorption capacity of the investigated cations is shown in Fig. 19. While, thorium adsorption was only partially inhibited by U(VI), the Ni^{2+} and Cu^{2+} did not inhibit uptake. Where uptake was inhibited by U(VI), the effects were not large enough to prevent the

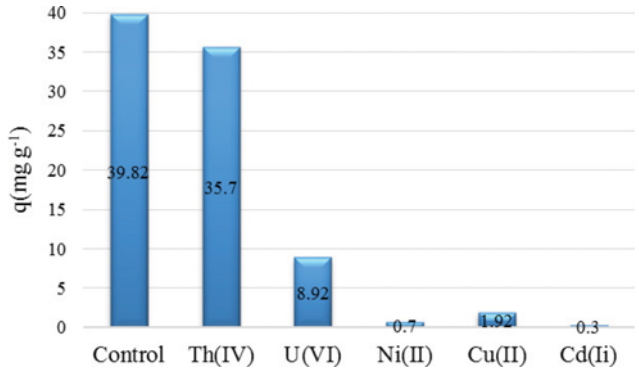

Fig. 19. Adsorption capacity of $TiSiNH_2$ for Th(IV) ions from the real sample solution (UCF waste-water sample) (adsorbent dosage of 3.89 gL^{-1}, temperature of 318 K, equilibrium time of 1,200 min and shaker speed, 150 rpm).

possible application of $TiSiNH_2$ as an adsorbent of thorium from aqueous solutions in its presence.

CONCLUSIONS

The adsorption of Th(IV) ions using functionalized titanosilicate matrix ($TiSiNH_2$) was investigated. The equilibrium, kinetics, and thermodynamics aspects of the adsorption were then evaluated. In the equilibrium study, the results indicated that the adsorption process fits very well with the mathematical model of the Langmuir in the studied concentration range, and the maximum monolayer adsorption capacity determined by Langmuir model was 87.71 mg g^{-1} which is in very good agreement with the experimental value (83.4 mg g^{-1}). Time-based investigations revealed that the double exponential model provides better correlation of the sorption data than the pseudo-first-order, pseudo-second-order and intra-particle models. The intraparticle diffusion is not the only rate control step, but also other processes may control the rate of sorption. The values of thermodynamic parameters were determined and the overall adsorption process was found to be physisorption, spontaneous and endothermic. Based on the obtained results, the functionalized titanosilicate matrix TiSiNH2 constitutes a good adsorbent for removing Th(IV) ions from the aqueous systems for the environmental protection purpose.

ACKNOWLEDGEMENTS

The authors would like to acknowledge the Jaberebne Hayan Research labs, Nuclear Science and Technology Research Institute (Tehran-Iran), for their support and contribution to this study.

REFERENCES

1. T. Y. Kim, S.-K. Park, S.-Y. Cho, H.-B. Kim, Y. Kang, S.-D. Kim

Table 5. Concentration of metal ions in waste-water sample from uranium conversion facility (UCF), Esfahan, Iran

Cation	U(VI)	Ni(II)	Cu(II)	Fe(III)	Mn(II)	Pb(II)	Cd(II)	Ca(II)	Mg(II)
Concentration (mg L^{-1})	28.76	22.12	12.63	0.01	0.02	0.05	0	2.74	0.02

and S.-J. Kim, *Korean J. Chem. Eng.*, **22**, 91 (2005).
2. B. C. Son, K. Park, S. H. Song and Y. Je Yoo, *Korean J. Chem. Eng.*, **21**, 1168 (2004).
3. H. C. Hahm, D. W. Lee, W. H. Hong, T.-y. Lee and C. H. Lee, *Korean J. Chem. Eng.*, **20**, 716 (2003).
4. M. Eskandari Nasab, A. Sam and A. A. Milani, *Hydrometallurgy*, **106**, 141 (2011).
5. M. Soylak and N. D. Erdogan, *J. Hazard. Mater.*, **137**, 1035 (2006).
6. M. M. Matlock, B. S. Howerton and D. A. Atwood, *Water Res.*, **36**, 4757 (2002).
7. S. Prabhakar, B. M. Misra, S. B. Roy, A. M. Meghal and T. K. Mukherjee, *Sep. Sci. Technol.*, **29**, 1001 (1994).
8. H. A. Qdais and H. Moussa, *Desalination*, **164**, 105 (2004).
9. B. Schlichter, V. Mavrov, T. Erwe and H. Chmiel, *J. Membr. Sci.*, **232**, 99 (2004).
10. B. R. Fillipi, J. F. Scamehorn, S. D. Christian and R. W. Taylor, *J. Membr. Sci.*, **145**, 27 (1998).
11. P. Cañizares, A. Ä. Pérez and R. Camarillo, *Desalination*, **144**, 279 (2002).
12. I. M. El-Naggar, K. A. Hebash, E. S. Sheneshen and E. A. Abdel-Galil, *ICAIJ*, **9**, 1 (2014).
13. I. M. El-Naggar, E. S. Sheneshen and E. A. Abdel-Galil, *Desalination Water Treatment*, **1**, 1 (2014).
14. F. A. Aydin and M. Soylak, *J. Hazard. Mater.*, **173**, 669 (2010).
15. A. G. El Samrani, B. S. Lartiges and F. Villiéras, *Water Res.*, **42**, 951 (2008).
16. P. Rule, K. Balasubramanian and R. R. Gonte, *J. Environ. Radioact*, **136**, 22 (2014).
17. D. L. Guerra, R. R. Viana and C. Airoldi, *J. Braz. Chem. Soc.*, **20**, 1164 (2009).
18. M. Metaxas, V. Kasselouri-Rigopoulou, P. Galiatsatou, C. Konstantopoulou and D. Oikonomoua, *J. Hazard. Mater.*, **97**, 71 (2003).
19. Z. Hongxia, D. Zheng and T. Zuyi, *Colloids Surf. A Physicochem Eng. Asp.*, **278**, 46 (2006).
20. C. Chen and X. Wang, *Appl. Radiat Isot.*, **65**, 155 (2007).
21. D. L. Zhao, S. J. Feng, C. L. Chen, S. H. Chen and D. Xu, *Appl. Clay Sci.*, **41**, 17 (2007).
22. A. Nilchi, T. Shariati Dehaghan and S. Rasouli Garmarodi, *Desalination*, **32**, 67 (2013).
23. S. K. Kazy, S. F. D'Souza and P. Sar, *J. Hazard. Mater.*, **163**, 65 (2009).
24. K. C. Bhainsa and S. F. D'Souza, *J. Hazard. Mater.*, **165**, 670 (2009).
25. Z. Talip, M. Eral and U. Hiçsönmez, *J. Environ. Radioact*, **100**, 139 (2009).
26. K. Popa, C. Claudiu and C. Pavel, *Desalination*, **293**, 78 (2012).
27. G. C. Panda, S. K. Das and A. K. Guha, *Colloids Surf. B Biointerfaces*, **62**, 173 (2008).
28. B. Tanchuk, J. A. Sawada and S. M. Kuznicki, *AIChE J.*, **59**, 12 (2013).
29. L. Marc, E. H. de Faria, M. Saltarelli, P. S. Calefi, E. J. Nassar and K. J. Ciuffi, *Ind. Eng. Chem. Res.*, **50**, 239 (2011).
30. M. Anbia, F. Khosravi and R. Dehghan, *J. Ultrafine Grained Nanostructured Mater.*, **49**, 36 (2016).
31. V. Kostov-Kytin, B. Mihailova, Y. Kalvachev and M. Tarassov, *Micropor. Mesopor. Mater.*, **86**, 223 (2005).
32. R. Saravanan and M. Prema Rani, Metal and Alloy Bonding: An Experimental Analysis-Charge Density in Metals and Alloys, Springer (2012).
33. A. Patterson, *Phys. Rev.*, **56**, 978 (1939).
34. M. M. Dubinin, Characterisation of Porous Solids. London: The Society of Chemical Industry (1979).
35. A. P. Terzyk, P. A. Gauden and P. Kowalczyk, *Carbon*, **40**, 2879 (2002).
36. I. Rahman, M. Jafarzadeh and C. Sipaut, *Ceramics International*, **35**, 1883 (2009).
37. A. M. McDonald and G. Y. Chao, *The Canadian Mineralogist*, **42**, 769 (2004).
38. V. Kostov-Kytin, B. Mihailova and Yu. Kalvachev, *Micropor. Mesopor. Mater.*, **86**, 223 (2005).
39. L. L. F. Su and X. Zhao, *J. Porous Mater.*, **13**, 263 (2006).
40. M. Anbia and M. Lashgari, *Chem. Eng. J.*, **150**, 555 (2009).
41. V. K. Gupta, B. Gupta, A. Rastogi, S. Agarwal and A. Nayak, *J. Hazard. Mater.*, **186**, 891 (2011).
42. V. K. Gupta, A. Mittal, A. Malviya and J. Mittal, *J. Colloid. Interface Sci.*, **355**, 24 (2009).
43. Y. H. Li, Z. Luan, X. Xiao, X. Zhou, C. Xu, D. Wu and B. Wei, *Adsorption Sci. Technol.*, **21**, 475 (2003).
44. E. I. Unuabonah, K. O. Adebowale, B. I. Olu-Owolabi, L. Z. Yang and L. X. Kong, *Hydrometallurgy*, **63**, 1 (2008).
45. Y. R. Huang, Z. J. Li, H. F. Wang, Z. C. Miao and J. G. Liu, *Appl. Chem. Ind.*, **38**, 1093 (2009).
46. S. Abbasizadeh, A. R. Keshtkar and M. A. Mousavian, *Chem. Eng. J.*, **220**, 161 (2013).
47. Y. S. Ho and G. Mckay, *Water Air Soil Pollut.*, **158**, 77 (2004).
48. Y. M. Hao, C. Man and Z. B. Hu, *J. Hazard. Mater.*, **184**, 392 (2010).
49. B. H. Hameed, D. K. Mahmoud and A. L. Ahmad, *J. Hazard. Mater.*, **158**, 65 (2008).
50. H. Zheng, D. Liua, Y. Zheng, S. Liang and Z. Liua, *J. Hazard. Mater.*, **167**, 141(2009).
51. H. Zheng, Y.Wang, Y. Zheng, H. Zhang, S. Liang and M. Long, *Chem. Eng. J.*, **143**, 117 (2008).
52. K. Saltalı, A. Sarı and M. Aydın, *J. Hazard. Mater.*, **141**, 258 (2007).
53. K. Saltalı and A. Sarı, *Adsorp. Sci. Technol.*, **24**, 749 (2006).
54. M. M. Dubinin, E. D. Zaverina and L. V. Radushkevich, *Zhurnal Fizicheskoi Khimii*, **21**, 1351 (1947).
55. Y. Sag and T. Kutsal, *Biochem. Eng. J.*, **6**, 145 (2000).
56. B. M. W. Trapnell and D. O. Hayward, Trapnell, Chemisorption, Butterworth, London (1964).